Coupled cavities for motional ground-state cooling and strong optomechanical coupling

Yong-Chun Liu,[1] Yun-Feng Xiao,[1,*] Xingsheng Luan,[2] Qihuang Gong,[1] and Chee Wei Wong[2,3,†]

[1]*State Key Laboratory for Mesoscopic Physics and School of Physics, Peking University; Collaborative Innovation Center of Quantum Matter, Beijing 100871, China*

[2]*Optical Nanostructures Laboratory, Columbia University, New York, New York 10027, USA*

[3]*Mesoscopic Optics and Quantum Electronics Laboratory, University of California, Los Angeles, California 90095, USA*

(Received 29 March 2014; published 16 March 2015)

Motional ground-state cooling and quantum-coherent manipulation of mesoscopic mechanical systems are crucial goals in both fundamental physics and applied science. We demonstrate that the motional ground state can be achieved in the highly unresolved sideband regime, through coherent auxiliary cavity interferences. We further illustrate coherent strong Rabi coupling between indirectly coupled and individually optimized mechanical resonators and optical cavities through effective dark-mode interaction. The proposed approach provides a platform for quantum manipulation of mesoscopic mechanical devices beyond the resolved sideband limit.

DOI: 10.1103/PhysRevA.91.033818 PACS number(s): 42.50.Wk, 07.10.Cm, 42.50.Lc

I. INTRODUCTION

Preparing mechanical quantum states free of thermal noise and with coherent manipulation is a crucial goal in cavity optomechanics [1–6]. Recently significant efforts on motional ground-state cooling have been mounted through dispersive coupling [7–15], along with recent theoretical efforts on dissipative coupling [16,17], dynamic cooling [18–22], atom-assisted cooling [23–25], and external cavity cooling [26]. Quantum noise, however, sets a fundamental limit for back-action cooling, and current dispersive ground-state cooling approaches must rely on the resolved sideband limit [27,28], requiring a cavity linewidth smaller than the single harmonic oscillator level spacing. In parallel, interference phenomena have been observed in optomechanical systems [29–32], including a mechanical mode interacting with two optical modes [33–39], with the application of coherent frequency conversion [40,41] and dark-mode observations [42] in the weak optomechanical coupling regime. For coherent exchange between optical and mechanical modes [43–46], however, a dramatically large optomechanical coupling rate exceeding that of optical decoherence has been deemed necessary. Conventionally, this poses a serious requirement for the optical Q factor, i.e., the good-cavity and resolved sideband limits.

Recently some approaches on ground-state cooling in the unresolved sideband regime [5] have been proposed. The dissipative coupling mechanism [16,17], parameter modulations [18–21], and hybrid system approaches [23–25,47] are shown to be capable of loosening resolved sideband conditions. However, experimental realization of these proposals are still difficult. Here we propose a practical coupled cavity system for both ground-state cooling of mechanical resonators and strong optomechanical coupling in the highly unresolved sideband condition, without requiring the coupled cavities in the normal mode splitting regime. We harness the destructive quantum interference in the all-optical domain of the coupled cavity system to achieve these goals. We find that ground-state cooling is realizable for a large range of cavity decay rates by coherently coupling to an auxiliary optical resonator or mode, which does not directly interact with the mechanical mode. We use effective dark-mode interaction model to analytically describe the system and demonstrate quantum-coherent coupling between individually optimized mechanical resonators and optical cavities. This not only allows quantum manipulation of massive mesoscopic mechanical devices with low frequencies but also enables quantum effects in a general platform with optimized optical and mechanical properties.

II. SYSTEM MODEL

Figure 1(a) illustrates two coupled optical cavities. The first primary cavity supports the optical mode a_1 (frequency ω_1, decay rate κ_1) and the mechanical mode b (frequency ω_{m}, decay rate γ) with single-photon optomechanical coupling strength g, while the second auxiliary cavity supports the optical mode a_2 (frequency ω_2, decay rate κ_2) and does not interact with the mechanical mode b. The interaction between the two optical modes is denoted by the tunnel-coupling parameter J [33,48–55]. The continuous-wave input laser excites mode a_1 with driving strength Ω. In the frame rotating at input laser frequency ω_{in}, the system Hamiltonian reads $H = -\Delta_1 a_1^\dagger a_1 - \Delta_2 a_2^\dagger a_2 + \omega_{\mathrm{m}} b^\dagger b + g a_1^\dagger a_1 (b^\dagger + b) + (J a_1^\dagger a_2 + J^* a_2^\dagger a_1) + (\Omega^* a_1 + \Omega a_1^\dagger)$, where $\Delta_1 \equiv \omega_{\mathrm{in}} - \omega_1$ and $\Delta_2 \equiv \omega_{\mathrm{in}} - \omega_2$ are the detunings. After linearization, the multiphoton optomechanical coupling strength reads $G \equiv g\alpha_1$ with α_1 the average intracavity field of mode a_1.

The energy levels of the coupled system are depicted in Fig. 1(b), where a series of three-level configurations can be extracted. In Fig. 1(c), $|1\rangle$ represents a short-lived state with high decay rate κ_1, while $|2\rangle$ denotes a long-lived metastable state with a small decay rate κ_2. Destructive quantum interference occurs between the two different excitation pathways, from $|0\rangle \to |1\rangle$ directly and from $|0\rangle \to |1\rangle \to |2\rangle \to |1\rangle$ indirectly. This allows the heating process through the optical field to be potentially suppressed. Meanwhile, the cooling process is almost unaffected due to off-resonance interaction.

*yfxiao@pku.edu.cn; http://www.phy.pku.edu.cn/~yfxiao/

†Electronic address: cheewei.wong@ucla.edu

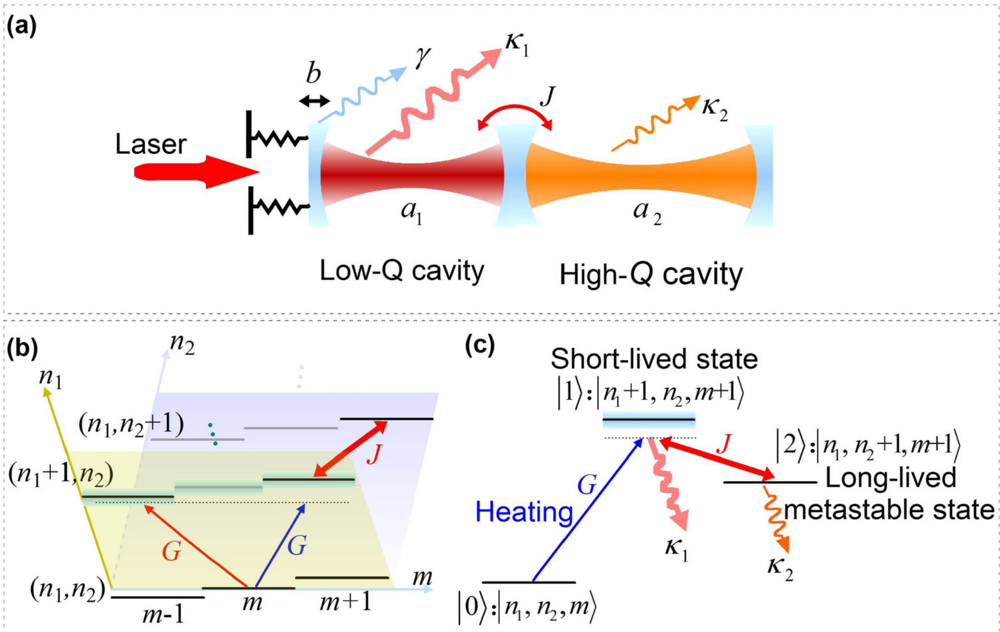

FIG. 1. (Color online) (a) Fabry-Pérot equivalent of the current system with two coupled optical cavities. The first cavity is a low-Q cavity and the second cavity is a high-Q cavity. The mechanical mode only interacts with the first cavity mode. (b) Energy level diagram of the system in the displaced frame. $|n_1,n_2,m\rangle$ denotes the state of n_1 photons in mode a_1, n_2 photons in mode a_2, and m phonons in mode b. The red (gray) double arrow denotes the coupling between states $|n_1+1,n_2,m+1\rangle$ and $|n_1,n_2+1,m+1\rangle$ with coupling strength J. (c) Energy levels forming the three-level configuration.

III. COOLING THROUGH COUPLED CAVITY INTERACTIONS BEYOND THE RESOLVED SIDEBAND LIMIT

To demonstrate the cooling, we derive and calculate the spectral density of the optical force using the quantum noise approach (see Appendix B),

$$S_{FF}(\omega) = \frac{|G|^2\kappa_1}{x_{\mathrm{ZPF}}^2}|\chi(\omega)|^2\left[1+\frac{\kappa_2}{\kappa_1}|J|^2|\chi_2(\omega)|^2\right], \quad (1)$$

where x_{ZPF} is the zero-point mechanical fluctuation, $\chi^{-1}(\omega) = \chi_1^{-1}(\omega)+J^2\chi_2(\omega)$, $\chi_1^{-1}(\omega)=-i(\omega+\Delta_1')+\kappa_1/2$, $\chi_2^{-1}(\omega) = -i(\omega+\Delta_2)+\kappa_2/2$, and $\Delta_1' = \Delta_1 + 2|G|^2/\omega_{\mathrm{m}}$ is the optomechanical-coupling modified detuning. Without the second optical mode a_2, the noise spectrum reduces to $S_{FF}^{(J=0)}(\omega) = |G|^2\kappa_1|\chi_1(\omega)|^2/x_{\mathrm{ZPF}}^2$, a Lorentzian noise spectrum. In the presence of mode a_2, $S_{FF}(\omega)$ becomes a complex lineshape due to interaction of the two optical modes. In Figs. 2(a) and 2(b) we plot the noise spectrum $S_{FF}(\omega)$ in the highly unresolved sideband regime $\kappa_1/\omega_{\mathrm{m}} = 10^4$ by examining various detunings Δ_1'. An asymmetric Fano (interference of a resonant scattering with continuum background) [56] lineshape or a symmetric narrow electromagnetically induced transparency (EIT, interference of two resonant scattering or optical transitions) [57–60] lineshape appears with sharp spectral change compared with the low-Q spectral background. This greatly increases the asymmetry between cooling and heating processes, with potential for enhanced cooling rate $A_- \equiv S_{FF}(\omega_{\mathrm{m}})x_{\mathrm{ZPF}}^2$ and suppressed heating rate $A_+ \equiv S_{FF}(-\omega_{\mathrm{m}})x_{\mathrm{ZPF}}^2$. Here A_- (A_+) represents the rate for absorbing (emitting) a phonon by the intracavity field, as illustrated in Figs. 2(c) and 2(d). In the single-cavity highly unresolved sideband regime, the cooling rate A_- and heating rate A_+ are almost the same, with net cooling rate $\Gamma_{\mathrm{opt}} \equiv A_- - A_+$ near zero [Figs. 2(c) and 2(e)]. In the presence of the second optical mode a_2, the quantum interference results in large suppression of A_+ while A_- is almost unchanged, leading to a very large net cooling rate Γ_{opt} [Figs. 2(d) and 2(f)]. Moreover, we note that the classical cooling limit $n_{\mathrm{f}}^{\mathrm{c}}$ ($\simeq\gamma n_{\mathrm{th}}/\Gamma_{\mathrm{opt}}$) is largely lowered, relaxing the requirement for initial cryogenic precooling; i.e., a higher bath thermal phonon number n_{th} can be tolerated. Furthermore, the quantum limit $n_{\mathrm{f}}^{\mathrm{q}}$ ($\simeq A_+/\Gamma_{\mathrm{opt}}$) is significantly reduced, breaking the resolved sideband requirement of backaction cooling. For the single-cavity case, the lowest achievable quantum limit, obtained for detuning $\Delta_1' = -\kappa_1/2$ in the unresolved sideband condition, is given by $\kappa_1/(4\omega_{\mathrm{m}})$. In the coupled cavity approach here, κ_1 is no longer a limit on the final phonon occupancy through cancellation of quantum backaction heating.

By solving the quantum master equation and employing the covariance approach (see Appendix C), exact numerical results are obtained, with an example time evolution of the mean phonon number presented in Fig. 2(g). In the presence of the second cavity the mean phonon occupancy is cooled from an initial 10^4 to below 1 even for highly unresolved sideband case $\kappa_1/\omega_{\mathrm{m}} = 10^4$, while in the absence of the second cavity, the mechanical motion cannot be cooled for such a large $\kappa_1/\omega_{\mathrm{m}}$.

Compared with the conventional single-cavity cooling case, a significant difference here is that the input laser can be blue detuned. In the quantum noise approach, the positive slope of $S_{FF}(\omega)$ is used for cooling while the negative slope corresponds to heating. For single cavity setup, positive slope of $S_{FF}(\omega)$ only appears on the left wing of the Lorentzian, while for coupled cavity system, the Fano or EIT

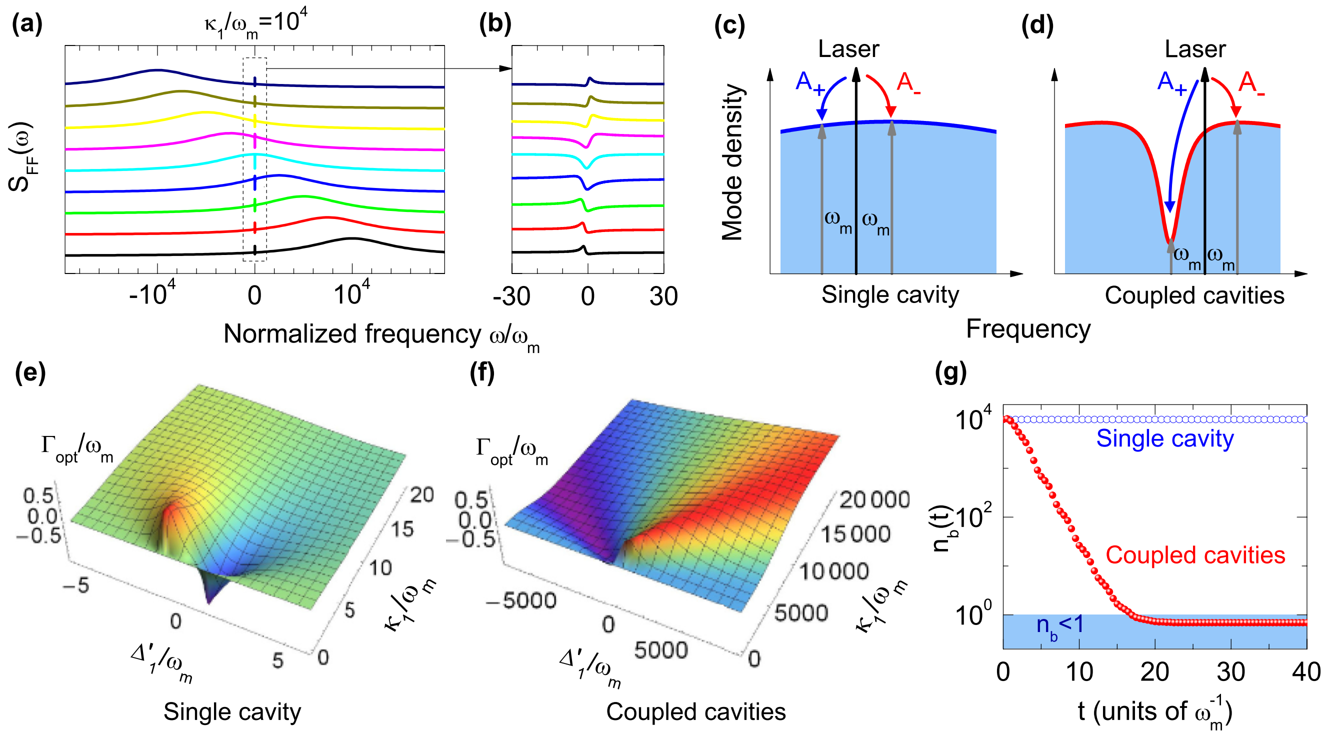

FIG. 2. (Color online) (a) Optical force spectrum $S_{FF}(\omega)$ for $\kappa_1/\omega_\mathrm{m} = 10^4$ and various Δ'_1. From top to bottom, Δ'_1 decreases from κ_1 to $-\kappa_1$ with step $0.25\kappa_1$. (b) View of the central one-fortieth of the dashed-box region in panel (a). [(c), (d)] Frequency domain interpretation of optomechanical interactions with a single cavity (c) and coupled cavities (d). The black vertical arrows denote the input laser, the gray vertical arrows denote the scattering sidebands, and the curved red (blue) arrows denote the anti-Stokes (Stokes) scattering processes A_- (A_+). [(e), (f)] Net optical cooling rate Γ_opt as functions of Δ'_1 and κ_1 for a single cavity (e) and coupled cavities (f). (g) Exact numerical results of the mean phonon number $n_b(t)$ for coupled cavities (red [gray] closed circles) with $\Delta'_1 = J^2/(\Delta_2 + \omega_\mathrm{m})$. The single-cavity case ($J = 0$) with $\Delta'_1 = -\kappa_1/2$ and $G/\omega_\mathrm{m} = 10$ is plotted for comparison (blue [gray] open circles). The shaded region denotes $n_b < 1$. Other unspecified parameters are $\kappa_1/\omega_\mathrm{m} = 10^4$, $\kappa_2/\omega_\mathrm{m} = 1$, $\Delta_2/\omega_\mathrm{m} = 0.5$, $J = \sqrt{\kappa_1\omega_\mathrm{m}}$, $G = 0.5J$, $\gamma/\omega_\mathrm{m} = 10^{-5}$, and $n_\mathrm{th} = 10^4$.

spectrum has rich structures. For example, the EIT lineshape can be viewed as an inverse Lorentzian lineshape. In Fig. 3(a) we plot exact numerical results of the steady-state final phonon number n_f as a function of two detunings Δ'_1 and Δ_2 for fixed intercavity interaction strength J. It shows optimal detunings are approximately described by $\Delta'_1(\Delta_2 + \omega_\mathrm{m}) = J^2$ (blue [gray] solid curve), calculated from Eq. (1) by maximizing the cooling rate A_-. In Figs. 3(b)–3(d) we plot $n_\mathrm{f} = n_\mathrm{f}^\mathrm{q} + n_\mathrm{f}^\mathrm{c}$, the quantum part n_f^q and classical part n_f^c as functions of Δ'_1 and Δ_2 for optimized intercavity interaction tuned by $J = \sqrt{\Delta'_1(\Delta_2 + \omega_\mathrm{m})}$ [along the blue [gray] solid curve in Fig. 3(a)]. It shows that ground-state cooling can be achieved for broad range of detunings. For the first cavity, this range exceeds $5 \times 10^4\omega_\mathrm{m}$; for the second cavity, significant cooling can be realized in the span of $-0.5 < \Delta_2/\omega_\mathrm{m} < 1$. In Fig. 3(c) the quantum limit n_f^q minimum is obtained for large Δ'_1 and negative Δ_2 (for Fano-like lineshapes), from a small quantum backaction heating $\propto S_{FF}(-\omega_\mathrm{m})$. On the other hand, the classical limit n_f^c minimum is achieved for small Δ'_1 and positive Δ_2 near $\Delta_2/\omega_\mathrm{m} \sim 1$ (for EIT-like lineshapes), which leads to a large cooling rate $\propto S_{FF}(\omega_\mathrm{m})$. The balance between these two limits lead to an optimal $\Delta'_1/\kappa_1 \sim 3$ and $\Delta_2/\omega_\mathrm{m} \sim 0.3$ for the parameters in Fig. 3(b).

Figures 3(e) and 3(f) demonstrates the broad parameter space for ground-state cooling in the unresolved sideband limit. With optimized couplings J and G, the final phonon number n_f for different ratios $\kappa_1/\omega_\mathrm{m}$ up to 10^6 are almost the same, which reveals that, arising from the unique interferences, the first cavity decay only acts as a background and has negligible influence on cooling for such large optical damping case. Figure 3(f) shows that for $\kappa_2/\omega_\mathrm{m} = 0.5$, the tolerable initial bath phonon number n_th is up to 3×10^4 (green [gray] triangles), corresponding to $T = 288$ K for $\omega_\mathrm{m}/2\pi = 200$ MHz, readily available in physical measurements.

IV. EFFECTIVE DARK-MODE INTERACTIONS: ANALYTICAL COOLING LIMITS, STRONG COUPLING, AND DYNAMICAL STABILITY

A. Analytical cooling limits

To gain more physical insights into the coupled cavity optomechanical system, we analyze the eigenmodes of the system. For large detuning, two of the system's eigenmodes are linear combinations of the mechanical mode and the high-Q cavity mode a_2; i.e., they are dark modes with respect to the low-Q cavity mode a_1. This dark-mode doublet can be considered as a result of the effective interaction between the mechanical mode and the high-Q mode a_2. The interaction is concisely described by the effective parameters

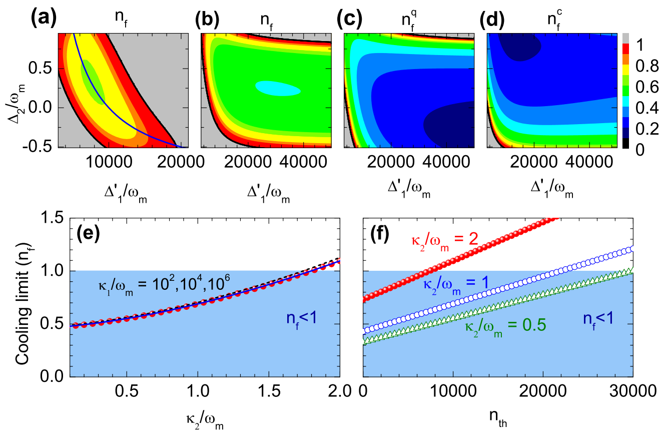

FIG. 3. (Color online) (a) Exact numerical results of the final phonon number n_{f} as functions of $\Delta_1'/\omega_{\mathrm{m}}$ and $\Delta_2/\omega_{\mathrm{m}}$ for $J/\omega_{\mathrm{m}} = 100$, $G = 0.5J$. The blue (gray) curve corresponds to $\Delta_1'(\Delta_2 + \omega_{\mathrm{m}}) = J^2$. [(b)–(d)] Final phonon number n_{f} (b), its quantum part $n_{\mathrm{f}}^{\mathrm{q}}$ (c), and its classical part $n_{\mathrm{f}}^{\mathrm{c}}$ (d) as functions of $\Delta_1'/\omega_{\mathrm{m}}$ and $\Delta_2/\omega_{\mathrm{m}}$ for $J = \sqrt{\Delta_1'(\Delta_2 + \omega_{\mathrm{m}})}$ and $G = 0.5J$. In panels (a)–(d), $\kappa_1/\omega_{\mathrm{m}} = 10^4$ and $n_{\mathrm{th}} = 10^4$. The black curves denote that the phonon number is 1. [(e), (f)] Final phonon number n_{f} as a function of $\kappa_2/\omega_{\mathrm{m}}$ (e) and n_{th} (f). In panel (e), $n_{\mathrm{th}} = 10^4$, $\kappa_1/\omega_{\mathrm{m}} = 10^6$ (red [gray] closed circles), 10^4 (blue [gray] solid curve), and 10^2 (black dashed curve); in panel (f), $\kappa_1/\omega_{\mathrm{m}} = 10^4$, $\kappa_2/\omega_{\mathrm{m}} = 2$ (red [gray] closed circles), 1 (blue [gray] open circles), and 0.5 (green [gray] triangles). Other unspecified parameters are $J = \sqrt{\kappa_1\omega_{\mathrm{m}}}$, $G = 0.5J$, $\Delta_2/\omega_{\mathrm{m}} = 0.5$, $\Delta_1' = J^2/(\Delta_2 + \omega_{\mathrm{m}})$, and $\gamma/\omega_{\mathrm{m}} = 10^{-5}$. The shaded regions denote $n_{\mathrm{f}} < 1$.

(see Appendix D)

$$|G_{\mathrm{eff}}| = \eta|G|, \quad \kappa_{\mathrm{eff}} = \kappa_2 + \eta^2\kappa_1, \quad \Delta_{\mathrm{eff}} = \Delta_2 - \eta^2\Delta_1', \tag{2}$$

where η is the scaled intercavity coupling strength given by

$$\eta = \frac{|J|}{|\Delta_1'|} \tag{3}$$

for large detuning $|\Delta_1'| > \kappa_1$. Note that mode a_2 does not directly interact with mode b, and the indirect effective interaction is mediated by mode a_1 [Fig. 4(a) inset]. It reveals from Eq. (2) that the effective detuning Δ_{eff} is a combination of Δ_1' and Δ_2, uniquely allowing blue-detuned Δ_1' and Δ_2 to obtain a red-detuned Δ_{eff}. With the effective dark-mode interaction model, the cooling limits can be analytically described by (see Appendix D)

$$n_{\mathrm{f}}^{\mathrm{eff}} = \frac{\gamma n_{\mathrm{th}}}{\Gamma_{\mathrm{eff}}} + \frac{\kappa_{\mathrm{eff}}^2}{16\omega_{\mathrm{m}}^2}, \tag{4}$$

where $\Gamma_{\mathrm{eff}} = 4|G_{\mathrm{eff}}|^2/\kappa_{\mathrm{eff}}$ is the effective cooling rate. It reveals that ground-state cooling requires $\kappa_2 + \eta^2\kappa_1 \lesssim 4\omega_{\mathrm{m}}$, only slightly dependent on the first cavity decay rate κ_1 for $\eta \ll 1$. The ultimate limitation is the second cavity decay rate κ_2, which should be comparable to ω_{m}. Notably, since b is not directly coupled to a_2, the optical and mechanical properties of the whole system can be optimized individually, without simultaneous requirements in the same resonator. Particularly, the second cavity does not need to support any mechanical modes, and the only requirement is relatively high optical Q.

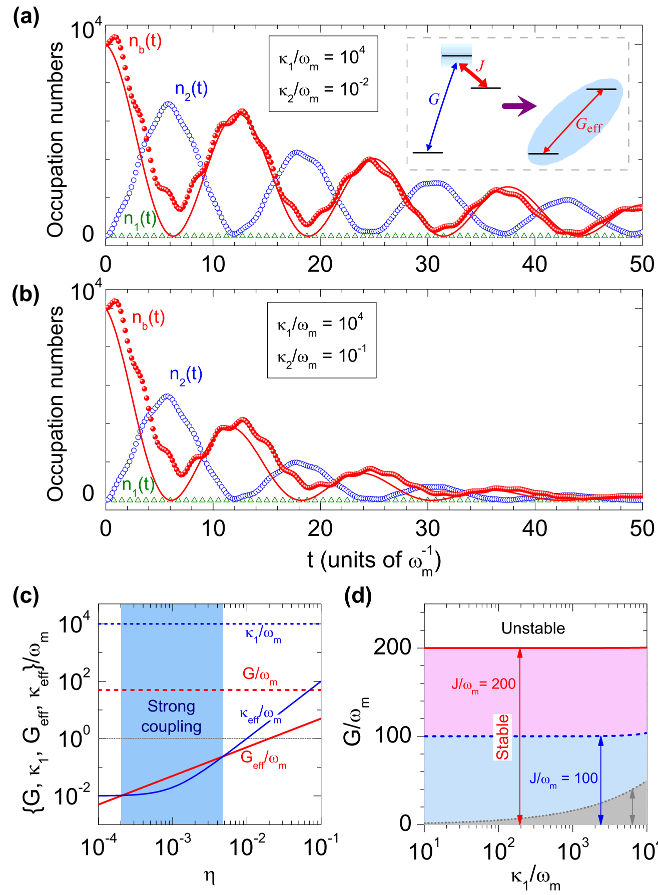

FIG. 4. (Color online) Exact numerical results of the mean phonon number $n_b(t)$ (red [gray] closed circles), mean photon numbers $n_2(t)$ (blue [gray] open circles), and $n_1(t)$ (green [gray] triangles) for $\kappa_1/\omega_{\mathrm{m}} = 10^4$, $J/\omega_{\mathrm{m}} = 200$, and $G = 0.5J$. (a) $\kappa_2/\omega_{\mathrm{m}} = 0.01$; (b) $\kappa_2/\omega_{\mathrm{m}} = 0.1$. The red [gray] solid curves are the analytical result for $n_b(t)$. Inset of panel (a): Schematic energy diagram of the effective dark-mode interaction. (c) Parameters G/ω_{m} (red [gray] dashed curve), $\kappa_1/\omega_{\mathrm{m}}$ (blue [gray] dashed curve), $G_{\mathrm{eff}}/\omega_{\mathrm{m}}$ (red [gray] solid curve), and $\kappa_{\mathrm{eff}}/\omega_{\mathrm{m}}$ (blue [gray] solid curve) as functions of η. The shaded region denotes $G_{\mathrm{eff}} > \kappa_{\mathrm{eff}}$. The gray dotted line denotes the value of 1 in the unit of ω_{m}. (d) Dynamical stable regions for coupled cavities with $J/\omega_{\mathrm{m}} = 200$ (below the red [gray] solid curve) and $J/\omega_{\mathrm{m}} = 100$ (below the blue [gray] dashed curve), and single-cavity case (below the gray dash-dotted curve). Other unspecified parameters are $\Delta_2/\omega_{\mathrm{m}} = -0.5$, $\Delta_1' = J^2/(\Delta_2 + \omega_{\mathrm{m}})$, $\gamma/\omega_{\mathrm{m}} = 10^{-5}$, and $n_{\mathrm{th}} = 10^4$. This parameter regime can be reached, for example, in coupled microtoroids with $\omega_{\mathrm{m}} = 100$ MHz, $J = 20$ GHz, $\kappa_2 = 1 \sim 10$ MHz [33].

B. Strong coupling

The current system also enables strong coupling between mode a_2 and mode b even when mode a_1 is highly dissipative, with the similar mechanism of strong-coupling cavity quantum electrodynamics in highly dissipative cavities [61]. Figures 4(a) and 4(b) shows that Rabi oscillation occurs for modes a_2 and b with $\kappa_1/\omega_{\mathrm{m}} = 10^4$. It reveals reversible energy exchange between these two indirectly coupled modes, with decoherence time much longer than the coherent exchange period. Note that the analytical results (red [gray] solid curve) calculated from the effective dark-mode interaction model (see

Appendix D) agree well with the exact numerical results. In this case the effective strong coupling condition $|G_{\mathrm{eff}}| > \kappa_{\mathrm{eff}}$ is satisfied. As shown in Eq. (2) and Fig. 4(c), for $\eta \ll 1$, both the effective coupling strength $|G_{\mathrm{eff}}|$ and effective cavity decay rate κ_{eff} are smaller than the original $|G|$ and κ_1, respectively. However, κ_{eff} decreases more rapidly than $|G_{\mathrm{eff}}|$ for decreasing η. Therefore, strong coupling regime can be reached, corresponding to the shaded region in Fig. 4(c). From Eq. (2), it can be obtained that the strong coupling condition is relaxed to $|G| > 4\kappa_1\kappa_2$. For parameters examined in Fig. 4(a), we obtain $\eta = 2.5 \times 10^{-3}$, $G_{\mathrm{eff}}/\omega_{\mathrm{m}} = 0.25$, $\kappa_{\mathrm{eff}}/\omega_{\mathrm{m}} = 0.07$, and $\Delta_{\mathrm{eff}}/\omega_{\mathrm{m}} = -1$. With $n_{\mathrm{th}} = 2 \times 10^4$, we find $G_{\mathrm{eff}} > (\kappa_{\mathrm{eff}}, \gamma n_{\mathrm{th}})$, which is in the quantum-coherent coupling regime. This establishes an efficient quantum interface between the mechanical resonator and the photons and allows the control of the mechanical quantum states.

C. Dynamical stability

To examine the dynamical stability of the coupled-mode optomechanical interactions, we calculate the stable regions through the Routh-Hurwitz criterion (see Appendix E) as presented in Fig. 4(d). It reveals that large optomechanical coupling G can be allowed to keep the system in the stable region, and it is more stable than the single cavity case, because the intercavity coupling provides additional restoring force to the mechanical oscillator. With the large allowed $|G|$, the effective coupling strength $|G_{\mathrm{eff}}|$ far exceeds the effective decay rate κ_{eff}, bringing the system deeply in the strong coupling regime.

V. CONCLUSIONS

In summary, we have proposed the harnessing of coupled cavity interferences and dark-mode interaction for ground-state cooling of mechanical resonators and strong quantum-coherent optomechanical coupling beyond the resolved sideband limit. Through destructive quantum interferences, we demonstrate that the coupled cavity system not only significantly accelerates the cooling process but also dramatically reduces the cooling limits. Ground-state cooling is achievable for large cavity decay rate κ_1 when the coupled auxiliary cavity has modest decay rate $\kappa_2 \sim \omega_{\mathrm{m}}$. The auxiliary cavity mode is not directly coupled to the mechanical mode, allowing individual optimization of the optical and mechanical properties. Therefore, the first cavity only needs to possess good mechanical properties while the second cavity only needs to possess relatively high optical Q. Unlike the dissipative coupling mechanism [16,17], we use pure dispersive coupling and all-optical EIT effect to realize destructive interference, and the interference comes from two resonant contributions. Note that the cavity decay rate in our case is the total decay rate where the intrinsic decay rate has been taken into account. This is important because in real experiments the external decay rate is usually tunable while the intrinsic cavity decay rate is the fundamental limitation. Unlike the proposal using two-level atomic ensembles [23] and precooled atoms [25], our approach makes use of pure cavity optomechanical cooling effect arising from dynamical backaction, and it is quite practical in experimental realization, for instance, in a photonic crystal cavity system with highly unresolved sideband condition [62]. With dark-mode interaction in the strong coupling regime, the coupled cavity system allows for quantum-coherent coupling between mechanical mode and auxiliary cavity modes, with potential for quantum network applications [63–65]. This system establishes an efficient quantum interface between indirectly coupled and individually optimized mechanical resonators and optical cavities, which opens up the possibility for application of cavity quantum optomechanics beyond the resolved sideband regime, addressing the restricted experimental bounds at present.

ACKNOWLEDGMENTS

We thank Jing Shu and Zhang-qi Yin for discussions. This work was supported by Defense Advanced Research Projects Agency ORCHID program (C11L10831), 973 Program (No. 2013CB328704, No. 2013CB921904), National Natural Science Foundation of China (No. 61435001, No. 11474011, No. 11222440, No. and 11121091), and RFDPH (No. 20120001110068).

APPENDIX A: SYSTEM HAMILTONIAN AND QUANTUM LANGEVIN EQUATIONS

The Hamiltonian of the coupled cavity system is given by

$$H = H_{\mathrm{free}} + H_{\mathrm{o-m}} + H_{\mathrm{o-o}} + H_{\mathrm{drive}}. \tag{A1}$$

The first term H_{free} represents the free Hamiltonian of the optical and mechanical modes, described by $H_{\mathrm{free}} = \omega_1 a_1^\dagger a_1 + \omega_2 a_2^\dagger a_2 + \omega_{\mathrm{m}} b^\dagger b$, where ω_1, ω_2, and ω_{m} are the resonance frequencies of the first (or primary) cavity mode a_1, the second (or auxiliary) cavity mode a_2, and the mechanical mode b. The second term of Eq. (A1) ($H_{\mathrm{o-m}}$) describes the optomechanical interaction between the first cavity mode a_1 and the mechanical mode b, which is written as $H_{\mathrm{o-m}} = g a_1^\dagger a_1 (b^\dagger + b)$ [66], where g represents the single-photon optomechanical coupling strength. The third term of Eq. (A1) ($H_{\mathrm{o-o}}$) describes the coupling between the two cavity modes a_1 and a_2, with the Hamiltonian

$$H_{\mathrm{o-o}} = J a_1^\dagger a_2 + J^* a_2^\dagger a_1, \tag{A2}$$

where J describes the interaction strength [33,48–55]. The last term of Eq. (A1) (H_{drive}) describes the optical driving. Assume that the system is excited through simultaneous driving of the two cavity modes with the same input laser frequency ω_{in}. In this case the Hamiltonian is given by $H_{\mathrm{drive}} = (\Omega_1^* e^{i\omega_{\mathrm{in}} t} a_1 + \Omega_1 e^{-i\omega_{\mathrm{in}} t} a_1^\dagger) + (\Omega_2^* e^{i\omega_{\mathrm{in}} t} a_2 + \Omega_2 e^{-i\omega_{\mathrm{in}} t} a_2^\dagger)$, where $\Omega_1 = \sqrt{\kappa_1^{\mathrm{ex}} P_1/(\hbar\omega_{\mathrm{in}})} e^{i\phi_1}$ and $\Omega_2 = \sqrt{\kappa_2^{\mathrm{ex}} P_2/(\hbar\omega_{\mathrm{in}})} e^{i\phi_2}$ denote the driving strengths, $P_1\,(P_2)$ is the input power and $\phi_1\,(\phi_2)$ is the initial phase for the first (second) input laser, and $\kappa_1^{\mathrm{ex}}\,(\kappa_2^{\mathrm{ex}})$ is the input-cavity coupling rate for mode $a_1\,(a_2)$. Alternatively, the system can also be excited through single-mode driving of either cavity mode, corresponding to $\Omega_1 = 0$ or $\Omega_2 = 0$. This only affects the mean intracavity field of the two cavity modes and the equilibrium position of the mechanical resonator, while the quantum fluctuations and thereby the linearized quantum Langevin equations (see below) remain the same.

In the frame rotating at the input laser frequency $\omega_{\rm in}$, the Hamiltonian is written as $H = -\Delta_1 a_1^\dagger a_1 - \Delta_2 a_2^\dagger a_2 + \omega_{\rm m} b^\dagger b + g a_1^\dagger a_1 (b^\dagger + b) + (J a_1^\dagger a_2 + J^* a_2^\dagger a_1) + (\Omega_1^* a_1 + \Omega_1 a_1^\dagger) + (\Omega_2^* a_2 + \Omega_2 a_2^\dagger)$, where $\Delta_1 \equiv \omega_{\rm in} - \omega_1$, $\Delta_2 \equiv \omega_{\rm in} - \omega_2$ are the detunings.

The quantum Langevin equations are given by

$$\dot{a}_1 = \left(i\Delta_1 - \frac{\kappa_1}{2}\right)a_1 - iga_1(b^\dagger + b) - iJa_2 - i\Omega_1 - \sqrt{\kappa_1}a_{\rm in,1}, \tag{A3}$$

$$\dot{a}_2 = \left(i\Delta_2 - \frac{\kappa_2}{2}\right)a_2 - iJ^*a_1 - i\Omega_2 - \sqrt{\kappa_2}a_{\rm in,2}, \tag{A4}$$

$$\dot{b} = \left(-i\omega_{\rm m} - \frac{\gamma}{2}\right)b - iga_1^\dagger a_1 - \sqrt{\gamma}b_{\rm in}, \tag{A5}$$

where $\kappa_1 \equiv \omega_1/Q_1$, $\kappa_2 \equiv \omega_2/Q_2$, and $\gamma \equiv \omega_{\rm m}/Q_{\rm m}$ are the decay rates of the modes a_1, a_2, and b, respectively; Q_1, Q_2, and $Q_{\rm m}$ are the corresponding quality factors; and $a_{\rm in,1}$, $a_{\rm in,2}$, and $b_{\rm in}$ are the corresponding noise operators, which satisfy $\langle a_{\rm in,1}(t)a_{\rm in,1}^\dagger(t')\rangle = \langle a_{\rm in,2}(t)a_{\rm in,2}^\dagger(t')\rangle = \delta(t-t')$, $\langle a_{\rm in,1}^\dagger(t)a_{\rm in,1}(t')\rangle = \langle a_{\rm in,2}^\dagger(t)a_{\rm in,2}(t')\rangle = 0$, $\langle b_{\rm in}(t)b_{\rm in}^\dagger(t')\rangle = (n_{\rm th}+1)\delta(t-t')$, and $\langle b_{\rm in}^\dagger(t)b_{\rm in}(t')\rangle = n_{\rm th}\delta(t-t')$. Here $n_{\rm th}$ is the thermal phonon number given by $n_{\rm th}^{-1} = \exp(\frac{\hbar\omega_{\rm m}}{k_{\rm B}T}) - 1$, where T is the environmental temperature and $k_{\rm B}$ is Boltzmann constant.

Now we apply a displacement transformation $a_1 \to \alpha_1 + a_1$, $a_2 \to \alpha_2 + a_2$, $b \to \beta + b$, where α_1, α_2, and β are c numbers denoting the displacements of the optical and mechanical modes. The quantum Langevin equations are rewritten as

$$\dot{a}_1 = \left(i\Delta_1' - \frac{\kappa_1}{2}\right)a_1 - ig\alpha_1(b^\dagger + b) - iga_1(b^\dagger + b) - iJa_2 - \sqrt{\kappa_1}a_{\rm in,1}, \tag{A6}$$

$$\dot{a}_2 = \left(i\Delta_2 - \frac{\kappa_2}{2}\right)a_2 - iJ^*a_1 - \sqrt{\kappa_2}a_{\rm in,2}, \tag{A7}$$

$$\dot{b} = \left(-i\omega_{\rm m} - \frac{\gamma}{2}\right)b - ig\left(\alpha_1^* a_1 + \alpha_1 a_1^\dagger\right) - iga_1^\dagger a_1 - \sqrt{\gamma}b_{\rm in}, \tag{A8}$$

with the optomechanical-coupling modified detuning $\Delta_1' = \Delta_1 - g(\beta^* + \beta)$. Under strong driving conditions, the nonlinear terms $iga_1(b^\dagger + b)$ and $iga_1^\dagger a_1$ in the above equations are neglected. Then the quantum Langevin equations become linearized, and the linearized system Hamiltonian can be extracted as

$$H_L = -\Delta_1' a_1^\dagger a_1 - \Delta_2 a_2^\dagger a_2 + \omega_{\rm m} b^\dagger b + (Ga_1^\dagger + G^* a_1)(b^\dagger + b) + (Ja_1^\dagger a_2 + J^* a_2^\dagger a_1), \tag{A9}$$

where $G \equiv g\alpha_1$ is the coherent intracavity-field-enhanced optomechanical coupling strength.

APPENDIX B: QUANTUM NOISE APPROACH

From Eq. (A9) we obtain the optical force acting on the mechanical resonator $F = -(G^* a_1 + Ga_1^\dagger)/x_{\rm ZPF}$, where $x_{\rm ZPF} \equiv \sqrt{\hbar/(2m_{\rm eff}\omega_{\rm m})}$ is the zero-point fluctuation and $m_{\rm eff}$ is the effective mass of the mechanical resonator. The quantum noise spectrum of the optical force is given by the Fourier transform of the autocorrelation function $S_{FF}(\omega) \equiv \int dt e^{i\omega t}\langle F(t)F(0)\rangle$.

In the frequency domain, the operators $\tilde{a}_1(\omega)$, $\tilde{a}_2(\omega)$, and $\tilde{b}(\omega)$ obey

$$-i\omega\tilde{a}_1(\omega) = \left(i\Delta_1' - \frac{\kappa_1}{2}\right)\tilde{a}_1(\omega) - iG[\tilde{b}^\dagger(\omega) + \tilde{b}(\omega)] - iJ\tilde{a}_2(\omega) - \sqrt{\kappa_1}\tilde{a}_{\rm in,1}(\omega), \tag{B1}$$

$$-i\omega\tilde{a}_2(\omega) = \left(i\Delta_2 - \frac{\kappa_2}{2}\right)\tilde{a}_2(\omega) - iJ^*\tilde{a}_1(\omega) - \sqrt{\kappa_2}\tilde{a}_{\rm in,2}(\omega), \tag{B2}$$

$$-i\omega\tilde{b}(\omega) = \left(-i\omega_{\rm m} - \frac{\gamma}{2}\right)\tilde{b}(\omega) - i[G^*\tilde{a}_1(\omega) + G\tilde{a}_1^\dagger(\omega)] - \sqrt{\gamma}\tilde{b}_{\rm in}(\omega). \tag{B3}$$

Then we obtain

$$\tilde{b}(\omega) \simeq \frac{\sqrt{\gamma}\tilde{b}_{\rm in}(\omega) - i\sqrt{\kappa_1}A_1(\omega) - \sqrt{\kappa_2}A_2(\omega)}{i\omega - i[\omega_{\rm m} + \Sigma(\omega)] - \frac{\gamma}{2}}, \tag{B4}$$

where we have neglected $\tilde{b}^\dagger(\omega)$ terms and

$$A_1(\omega) = G^*\chi(\omega)\tilde{a}_{\rm in,1}(\omega) + G\chi^*(-\omega)\tilde{a}_{\rm in,1}^\dagger(\omega), \tag{B5}$$

$$A_2(\omega) = J[G^*\chi(\omega)\chi_2(\omega)\tilde{a}_{\rm in,2}(\omega) - G\chi^*(-\omega)\chi_2^*(-\omega)\tilde{a}_{\rm in2}^\dagger(\omega)], \tag{B6}$$

$$\Sigma(\omega) = -i|G|^2[\chi(\omega) - \chi^*(-\omega)], \tag{B7}$$

$$\chi(\omega) = \frac{1}{\frac{1}{\chi_1(\omega)} + |J|^2\chi_2(\omega)}, \tag{B8}$$

$$\chi_1(\omega) = \frac{1}{-i(\omega + \Delta_1') + \frac{\kappa_1}{2}}, \tag{B9}$$

$$\chi_2(\omega) = \frac{1}{-i(\omega + \Delta_2) + \frac{\kappa_2}{2}}, \tag{B10}$$

$$\chi_{\rm m}(\omega) = \frac{1}{-i(\omega - \omega_{\rm m}) + \frac{\gamma}{2}}, \tag{B11}$$

where $A_{1,2}(\omega)$ accounts for the contribution of the first and second cavities; $\Sigma(\omega)$ represents the optomechanical self energy; $\chi(\omega)$ is the total response function of the coupled cavities; and $\chi_1(\omega)$, $\chi_2(\omega)$, and $\chi_{\rm m}(\omega)$ are the response functions of the first cavity, the second cavity, and the mechanical mode. The optomechanical coupling-induced mechanical frequency shift $\delta\omega_{\rm m}$ and damping $\Gamma_{\rm opt}$ are given by $\delta\omega_{\rm m} = {\rm Re}\Sigma(\omega_{\rm m})$ and $\Gamma_{\rm opt} = -2\,{\rm Im}\Sigma(\omega_{\rm m})$.

By using $F(\omega) = -[G^* a_1(\omega) + G a_1^\dagger(\omega)]/x_{\mathrm{ZPF}}$, the spectral density of the optical force is obtained as

$$S_{FF}(\omega) = \frac{|G\chi(\omega)|^2}{x_{\mathrm{ZPF}}^2}[\kappa_1 + \kappa_2 |J|^2 |\chi_2(\omega)|^2]. \tag{B12}$$

This equation corresponds to Eq. (1) of the main text.

APPENDIX C: QUANTUM MASTER EQUATION AND COVARIANCE APPROACH

The quantum master equation of the system reads

$$\begin{aligned}\dot{\rho} &= i[\rho, H_L] + \frac{\kappa_1}{2}(2a_1\rho a_1^\dagger - a_1^\dagger a_1 \rho - \rho a_1^\dagger a_1)\\ &\quad + \frac{\kappa_2}{2}(2a_2\rho a_2^\dagger - a_2^\dagger a_2\rho - \rho a_2^\dagger a_2)\\ &\quad + \frac{\gamma}{2}(n_{\mathrm{th}}+1)(2b\rho b^\dagger - b^\dagger b\rho - \rho b_1^\dagger b_1)\\ &\quad + \frac{\gamma}{2} n_{\mathrm{th}}(2b^\dagger \rho b - bb^\dagger \rho - \rho bb^\dagger),\end{aligned} \tag{C1}$$

where H_L is the linearized system Hamiltonian given by Eq. (A9).

To calculate time evolutions of the mean phonon number $n_b(t) = \langle b^\dagger b\rangle(t)$, we need to determine the mean values of all the time-dependent second-order moments, $\langle a_1^\dagger a_1\rangle$, $\langle a_2^\dagger a_2\rangle$, $\langle b^\dagger b\rangle$, $\langle a_1^\dagger a_2\rangle$, $\langle a_1^\dagger b\rangle$, $\langle a_2^\dagger b\rangle$, $\langle a_1 a_2\rangle$, $\langle a_1 b\rangle$, $\langle a_2 b\rangle$, $\langle a_1^2\rangle$, $\langle a_2^2\rangle$, and $\langle b^2\rangle$, which are determined by a linear system of ordinary differential equations $\partial_t\langle \hat{o}_i \hat{o}_j\rangle = \mathrm{Tr}(\dot{\rho}\hat{o}_i\hat{o}_j) = \sum_{k,l}\eta_{k,l}\langle \hat{o}_k \hat{o}_l\rangle$, where $\hat{o}_i$, $\hat{o}_j$, $\hat{o}_k$, and $\hat{o}_l$ are one of the operators $a_1, a_2, b, a_1^\dagger, a_2^\dagger$, and $b_1^\dagger$, and $\eta_{k,l}$ are the corresponding coefficients determined by Eq. (C1) [22]. Initially, the mean phonon number is equal to the bath thermal phonon number, i.e., $\langle b^\dagger b\rangle(t=0) = n_{\mathrm{th}}$, and other second-order moments are zero. The numerical results in the main text are obtained by solving these differential equations.

APPENDIX D: EFFECTIVE DARK-MODE INTERACTION

The second cavity mode a_2 does not directly interact with the mechanical mode b. However, there exists indirect interaction between them, which is mediated by the first cavity mode a_1. From Eqs. (A6)–(A8), after neglecting the nonlinear terms, we obtain the formally integrated form for the operators as

$$\begin{aligned}a_1(t) &= a_1(0)\exp\left(i\Delta_1' t - \frac{\kappa_1}{2}t\right) + \exp\left(i\Delta_1' t - \frac{\kappa_1}{2}t\right)\\ &\quad\times\int_0^t[-iGb(\tau) - iGb^\dagger(\tau) - iJa_2(\tau) - \sqrt{\kappa_1}a_{\mathrm{in},1}(\tau)]\\ &\quad\times\exp\left(-i\Delta_1\tau + \frac{\kappa_1}{2}\tau\right)d\tau,\end{aligned} \tag{D1}$$

$$\begin{aligned}a_2(t) &= a_2(0)\exp\left(i\Delta_2 t - \frac{\kappa_2}{2}t\right) + \exp\left(i\Delta_2 t - \frac{\kappa_2}{2}t\right)\\ &\quad\times\int_0^t\left[-iJ^* a_1(\tau) - \sqrt{\kappa_2}a_{\mathrm{in},2}(\tau)\right]\\ &\quad\times\exp\left(-i\Delta_2\tau + \frac{\kappa_2}{2}\tau\right)d\tau,\end{aligned} \tag{D2}$$

$$\begin{aligned}b(t) &= b(0)\exp\left(-i\omega_{\mathrm{m}} t - \frac{\gamma}{2}t\right) + \exp\left(-i\omega_{\mathrm{m}} t - \frac{\gamma}{2}t\right)\\ &\quad\times\int_0^t[-iG^* a_1(\tau) - iGa_1^\dagger(\tau) - \sqrt{\gamma}b_{\mathrm{in}}(\tau)]\\ &\quad\times\exp\left(i\omega_{\mathrm{m}}\tau + \frac{\gamma}{2}\tau\right)d\tau,\end{aligned} \tag{D3}$$

By considering the effects of mode a_1 as perturbations, and solving Eqs. (D2) and (D3), we obtain

$$a_2(t) \simeq a_2(0)\exp\left(i\Delta_2 t - \frac{\kappa_2}{2}t\right) + A_{\mathrm{in},2}(t), \tag{D4}$$

$$b(t) \simeq b(0)\exp\left(-i\omega_{\mathrm{m}} t - \frac{\gamma}{2}t\right) + B_{\mathrm{in}}(t), \tag{D5}$$

where $A_{\mathrm{in},2}(t)$ and $B_{\mathrm{in}}(t)$ denote the noise terms. By plugging Eqs. (D4) and (D5) into Eq. (D1) and with the condition $|\Delta_1| \gg |\Delta_2|$, $\kappa_1 \gg (\kappa_2,\gamma)$, we obtain

$$\begin{aligned}a_1(t) &\simeq -\frac{iG\left[b(t)+b^\dagger(t)\right]}{-i\Delta_1 + \frac{\kappa_1}{2}} - \frac{iJa_2(t)}{-i\Delta_1 + \frac{\kappa_1}{2}}\\ &\quad + a_1(0)\exp\left(i\Delta_1 t - \frac{\kappa_1}{2}t\right) + A_{\mathrm{in},1}(t),\end{aligned} \tag{D6}$$

where the noise term is denoted by $A_{\mathrm{in},1}(t)$. By neglecting the fast decaying term containing $\exp(-\kappa_1 t/2)$ and plugging the expression back to Eqs. (A7) and (A8), we compare the equations with the effective single-cavity case and obtain

$$i\Delta_2 - \frac{\kappa_2}{2} + \frac{|J|^2}{i\Delta_1' - \frac{\kappa_1}{2}} \longleftrightarrow i\Delta_{\mathrm{eff}} - \frac{\kappa_{\mathrm{eff}}}{2}, \tag{D7}$$

$$\left|\frac{J^* G}{i\Delta_1' - \frac{\kappa_1}{2}}\right| \longleftrightarrow |G_{\mathrm{eff}}|, \tag{D8}$$

where G_{eff} is the effective coupling strength, κ_{eff} is the effective decay rate of the optical cavity mode, and Δ_{eff} is the effective detuning between the input light and the optical resonance. Then the indirect interaction between mode a_2 and mode b can be described by the effective parameters $|G_{\mathrm{eff}}| = \eta|G|$, $\kappa_{\mathrm{eff}} = \kappa_2 + \eta^2\kappa_1$ and $\Delta_{\mathrm{eff}} = \Delta_2 - \eta^2\Delta_1'$ with $\eta = |J|/[\Delta_1'^2 + (\kappa_1/2)^2]^{1/2} \simeq |J|/|\Delta_1'|$ for $|\Delta_1'| > \kappa_1$. These correspond to Eqs. (2) and (3) of the main text.

From these effective parameters, we obtain the effective spectral density of optical force as

$$S_{FF}^{\mathrm{eff}}(\omega) = \frac{\kappa_{\mathrm{eff}}|G_{\mathrm{eff}}\chi_{\mathrm{eff}}(\omega)|^2}{x_{\mathrm{ZPF}}^2}, \tag{D9}$$

where we have defined the effective response function

$$\chi_{\mathrm{eff}}(\omega) = \frac{1}{-i(\omega + \Delta_{\mathrm{eff}}) + \frac{\kappa_{\mathrm{eff}}}{2}}. \tag{D10}$$

In Fig. 5 the comparison between $S_{FF}^{\mathrm{eff}}(\omega)$ [Eq. (B12)] and $S_{FF}^{\mathrm{eff}}(\omega)$ [Eq. (D9)] is displayed. It reveals that for the region near the Fano resonance, the effective optical force spectrum is a good approximation.

In the effective resolved sideband limit ($\omega_{\mathrm{m}} > \kappa_{\mathrm{eff}}$) and weak coupling regime ($\kappa_{\mathrm{eff}} > G_{\mathrm{eff}}$), the cooling limit reads

$$n_{\mathrm{f}}^{\mathrm{eff}} = \frac{\gamma n_{\mathrm{th}}}{\Gamma_{\mathrm{eff}}} + \frac{\kappa_{\mathrm{eff}}^2}{16\omega_{\mathrm{m}}^2}, \tag{D11}$$

where $\Gamma_{\mathrm{eff}} = 4|G_{\mathrm{eff}}|^2/\kappa_{\mathrm{eff}}$ is the effective cooling rate.

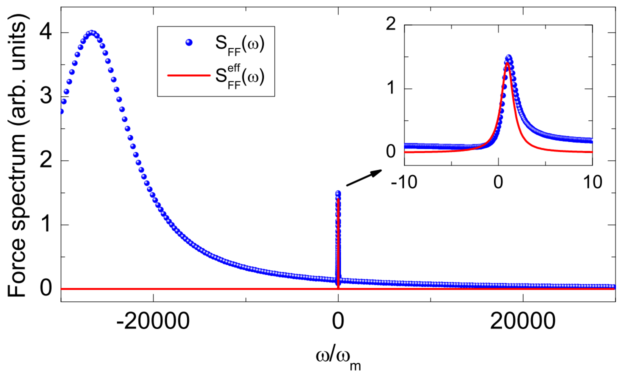

FIG. 5. (Color online) Optical force spectrum $S_{FF}(\omega)$ (blue [gray] dots) and $S_{FF}^{\rm eff}(\omega)$ (red [gray] solid curve) for $\kappa_1/\omega_{\rm m} = 10^4$, $\kappa_2/\omega_{\rm m} = 1$, $\Delta_2/\omega_{\rm m} = 0.5$, $J/\omega_{\rm m} = 200$, $G = 0.5J$, $\Delta_1' = |J|^2/(\Delta_2 + \omega_{\rm m})$, $\gamma/\omega_{\rm m} = 10^{-5}$, and $n_{\rm th} = 10^4$. The inset is a closeup view of the Fano region.

After eliminating mode a_1, the effective system Hamiltonian is given by

$$H_{\rm eff} = -\Delta_{\rm eff} a_2^\dagger a_2 + \omega_{\rm m} b^\dagger b + (G a_2^\dagger + G^* a_2)(b + b^\dagger). \tag{D12}$$

Then the quantum master equation reads

$$\begin{aligned}\dot\rho = {}& i[\rho, H_{\rm eff}] + \frac{\kappa_{\rm eff}}{2}(2a_2\rho a_2^\dagger - a_2^\dagger a_2\rho - \rho a_2^\dagger a_2)\\ &+ \frac{\gamma}{2}(n_{\rm th}+1)(2b\rho b^\dagger - b^\dagger b\rho - \rho b^\dagger b)\\ &+ \frac{\gamma}{2} n_{\rm th}(2b^\dagger\rho b - bb^\dagger\rho - \rho bb^\dagger).\end{aligned} \tag{D13}$$

By solving the differential equations of all the second-order moments relevant with modes a_2 and b [22,67], we obtain the time evolution of the mean phonon number in the effective strong coupling regime ($|G_{\rm eff}| > \kappa_{\rm eff}$) as

$$\begin{aligned} n_b(t) \simeq {}& n_{\rm th}\exp\left(-\frac{\kappa_{\rm eff}}{2}t\right)\cos^2(G_{\rm eff}t)\\ &+ \frac{\gamma n_{\rm th}}{\kappa_{\rm eff}} + \frac{8\,|G_{\rm eff}|^2 + \kappa_{\rm eff}^2}{16\omega_{\rm m}^2}.\end{aligned} \tag{D14}$$

The red (gray) dash-dotted curves in Figs. 4(a) and 4(b) of the main text are plotted according to this expression. Note that $n_b(t \to \infty) = \gamma n_{\rm th}/\kappa_{\rm eff} + (8|G_{\rm eff}|^2 + \kappa_{\rm eff}^2)/(16\omega_{\rm m}^2)$ corresponds to the cooling limit in the strong coupling regime. In our plots $n_{\rm th} \gg n_b(t \to \infty)$, so in Eq. (D14) we just simply add $n_b(t \to \infty)$ to the damped oscillation parts $n_{\rm th}\exp(-\kappa_{\rm eff}t/2)\cos^2(G_{\rm eff}t)$. In this case $n_b(0) \simeq n_{\rm th}$ can be satisfied in Eq. (D14).

APPENDIX E: DYNAMICAL STABILITY CONDITION

For the single-cavity case, the dynamical stability condition is given by

$$\Delta_1'\left[16\Delta_1'\,|G|^2 + \left(4\Delta_1'^2 + \kappa_1^2\right)\omega_{\rm m}\right] < 0, \tag{E1}$$

which is calculated from the Routh-Hurwitz criterion [68]. In the resolved sideband regime, for $\Delta_1' = -\kappa_1/2$, inequality (E1) reduces to

$$|G|^2 < \frac{\kappa_1\omega_{\rm m}}{4}. \tag{E2}$$

For the coupled cavity case, with the now derived effective parameters, the dynamical stability condition reads $\Delta_{\rm eff}[16\Delta_{\rm eff}|G_{\rm eff}|^2 + (4\Delta_{\rm eff}^2 + \kappa_{\rm eff}^2)\omega_{\rm m}] < 0$. Assume that the effective optomechanical interaction is in the resolved sideband regime, with the detuning $\Delta_{\rm eff} = -\omega_{\rm m}$, the stability condition reduces to $|G_{\rm eff}|^2 < \omega_{\rm m}^2/4 + \kappa_{\rm eff}^2/16$, which corresponds to

$$|G|^2 < \frac{4\omega_{\rm m}^2 + (\kappa_2 + \eta^2\kappa_1)^2}{16\eta^2}. \tag{E3}$$

Define the right-hand side of the inequality as S, and then the minimum value of S is given by

$$S_{\rm min} = \frac{\kappa_1}{4}\sqrt{\omega_{\rm m}^2 + \frac{\kappa_2^2}{4}} + \frac{\kappa_1\kappa_2}{8}, \tag{E4}$$

which is obtained when $\eta = \eta_{\rm min} \equiv \sqrt[4]{4\omega_{\rm m}^2 + \kappa_2^2}/\sqrt{\kappa_1}$. It reveals that, for the coupled cavity system, even in the worst case it allows larger optomechanical coupling to keep the system in the stable region, compared with the single cavity system for $\Delta_1' = -\kappa_1/2$ [inequality (E2)]. In Fig. 4(d) of the main text, the gray shaded region is plotted according to inequality (E2), and the blue and red shaded regions denote inequality (E3) for $J/\omega_{\rm m} = 100$ and 200, respectively.

[1] T. Carmon, H. Rokhsari, L. Yang, T. J. Kippenberg, and K. J. Vahala, Temporal behavior of radiation-pressure-induced vibrations of an optical microcavity phonon mode, Phys. Rev. Lett. **94**, 223902 (2005).

[2] T. J. Kippenberg, H. Rokhsari, T. Carmon, A. Scherer, and K. J. Vahala, Analysis of radiation-pressure induced mechanical oscillation of an optical microcavity, Phys. Rev. Lett. **95**, 033901 (2005).

[3] T. J. Kippenberg and K. J. Vahala, Cavity optomechanics: Back-action at the mesoscale, Science **321**, 1172 (2008).

[4] M. Aspelmeyer, T. J. Kippenberg, and F. Marquardt, Cavity optomechanics, Rev. Mod. Phys. **86**, 1391 (2014).

[5] Y.-C. Liu, Y.-W. Hu, C. W. Wong, and Y.-F. Xiao, Review of cavity optomechanical cooling, Chin. Phys. B **22**, 114213 (2013).

[6] Y.-C. Liu and Y.-F. Xiao, Macroscopic mechanical systems are entering the quantum world, Natl. Sci. Rev. doi:10.1093/nsr/nwu050 (2014).

[7] J. D. Teufel, T. Donner, D. Li, J. W. Harlow, M. S. Allman, K. Cicak, A. J. Sirois, J. D. Whittaker, K. W. Lehnert, and R. W. Simmonds, Sideband cooling of micromechanical motion to the quantum ground state, Nature (London) **475**, 359 (2011).

[8] J. Chan, T. P. Mayer Alegre, A. H. Safavi-Naeini, J. T. Hill, A. Krause, S. Gröblacher, M. Aspelmeyer, and O. Painter, Laser

cooling of a nanomechanical oscillator into its quantum ground state, Nature (London) **478**, 89 (2011).

[9] S. Gigan, H. R. Böhm, M. Paternostro, F. Blaser, G. Langer, J. B. Hertzberg, K. C. Schwab, D. Bäuerle, M. Aspelmeyer, and A. Zeilinger, Self-cooling of a micromirror by radiation pressure, Nature (London) **444**, 67 (2006).

[10] O. Arcizet, P.-F. Cohadon, T. Briant, M. Pinard, and A. Heidmann, Radiation-pressure cooling and micromechanical instability of a micromirror, Nature (London) **444**, 71 (2006).

[11] A. Schliesser, R. Rivière, G. Anetsberger, O. Arcizet, and T. J. Kippenberg, Resolved-sideband cooling of a micromechanical oscillator, Nat. Phys. **4**, 415 (2008).

[12] S. Gröblacher, J. B. Hertzberg, M. R. Vanner, G. D. Cole, S. Gigan, K. C. Schwab, and M. Aspelmeyer, Demonstration of an ultracold micro-optomechanical oscillator in a cryogenic cavity, Nat. Phys. **5**, 485 (2009).

[13] Y.-S. Park and H. Wang, Resolved-sideband and cryogenic cooling of an optomechanical resonator, Nat. Phys. **5**, 489 (2009).

[14] A. Schliesser, O. Arcizet, R. Rivère, G. Anetsberger, and T. J. Kippenberg, Resolved-sideband cooling and position measurement of a micromechanical oscillator close to the Heisenberg uncertainty limit, Nat. Phys. **5**, 509 (2009).

[15] T. Rocheleau, T. Ndukum, C. Macklin, J. B. Hertzberg, A. A. Clerk, and K. C. Schwab, Preparation and detection of a mechanical resonator near the ground state of motion, Nature (London) **463**, 72 (2010).

[16] F. Elste, S. M. Girvin, and A. A. Clerk, Quantum noise interference and backaction cooling in cavity nanomechanics, Phys. Rev. Lett. **102**, 207209 (2009).

[17] A. Xuereb, R. Schnabel, and K. Hammerer, Dissipative optomechanics in a Michelson-Sagnac interferometer, Phys. Rev. Lett. **107**, 213604 (2011).

[18] Y. Li, L.-A. Wu, and Z. D. Wang, Fast ground-state cooling of mechanical resonators with time-dependent optical cavities, Phys. Rev. A **83**, 043804 (2011).

[19] J.-Q. Liao and C. K. Law, Cooling of a mirror in cavity optomechanics with a chirped pulse, Phys. Rev. A **84**, 053838 (2011).

[20] X. Wang, S. Vinjanampathy, F. W. Strauch, and K. Jacobs, Ultraefficient cooling of resonators: Beating sideband cooling with quantum control, Phys. Rev. Lett. **107**, 177204 (2011).

[21] S. Machnes, J. Cerrillo, M. Aspelmeyer, W. Wieczorek, M. B. Plenio, and A. Retzker, Pulsed laser cooling for cavity optomechanical resonators, Phys. Rev. Lett. **108**, 153601 (2012).

[22] Y.-C. Liu, Y.-F. Xiao, X. Luan, and C. W. Wong, Dynamic dissipative cooling of a mechanical oscillator in strong coupling optomechanics, Phys. Rev. Lett. **110**, 153606 (2013).

[23] C. Genes, H. Ritsch, and D. Vitali, Micromechanical oscillator ground-state cooling via resonant intracavity optical gain or absorption, Phys. Rev. A **80**, 061803(R) (2009).

[24] J. Restrepo, C. Ciuti, and I. Favero, Single-polariton optomechanics, Phys. Rev. Lett. **112**, 013601 (2014).

[25] B. Vogell, K. Stannigel, P. Zoller, K. Hammerer, M. T. Rakher, M. Korppi, A. Jöckel, and P. Treutlein, Cavity-enhanced long-distance coupling of an atomic ensemble to a micromechanical membrane, Phys. Rev. A **87**, 023816 (2013).

[26] A. Xuereb, T. Freegarde, P. Horak, and P. Domokos, Optomechanical cooling with generalized interferometers, Phys. Rev. Lett. **105**, 013602 (2010).

[27] I. Wilson-Rae, N. Nooshi, W. Zwerger, and T. J. Kippenberg, Theory of ground state cooling of a mechanical oscillator using dynamical backaction, Phys. Rev. Lett. **99**, 093901 (2007).

[28] F. Marquardt, J. P. Chen, A. A. Clerk, and S. M. Girvin, Quantum theory of cavity-assisted sideband cooling of mechanical motion, Phys. Rev. Lett. **99**, 093902 (2007).

[29] Q. Lin, J. Rosenberg, D. Chang, R. Camacho, M. Eichenfield, K. J. Vahala, and O. Painter, Coherent mixing of mechanical excitations in nano-optomechanical structures, Nat. Photon. **4**, 236 (2010).

[30] S. Weis, R. Rivière, S. Deléglise, E. Gavartin, O. Arcizet, A. Schliesser, and T. J. Kippenberg, Optomechanically induced transparency, Science **330**, 1520 (2010).

[31] A. H. Safavi-Naeini, T. P. M. Alegre, J. Chan, M. Eichenfield, M. Winger, Q. Lin, J. T. Hill, D. E. Chang, and O. Painter, Electromagnetically induced transparency and slow light with optomechanics, Nature (London) **472**, 69 (2011).

[32] G. S. Agarwal and S. Huang, Electromagnetically induced transparency in mechanical effects of light, Phys. Rev. A **81**, 041803(R) (2010).

[33] I. S. Grudinin, H. Lee, O. Painter, and K. J. Vahala, Phonon laser action in a tunable two-level system, Phys. Rev. Lett. **104**, 083901 (2010).

[34] M. Ludwig, A. H. Safavi-Naeini, O. Painter, and F. Marquardt, Enhanced quantum nonlinearities in a two-mode optomechanical system, Phys. Rev. Lett. **109**, 063601 (2012).

[35] Y.-D. Wang and A. A. Clerk, Using interference for high fidelity quantum state transfer in optomechanics, Phys. Rev. Lett. **108**, 153603 (2012).

[36] L. Tian, Adiabatic state conversion and pulse transmission in optomechanical systems, Phys. Rev. Lett. **108**, 153604 (2012).

[37] S. Barzanjeh, M. Abdi, G. J. Milburn, P. Tombesi, and D. Vitali, Reversible optical-to-microwave quantum interface, Phys. Rev. Lett. **109**, 130503 (2012).

[38] Y.-D. Wang and A. A. Clerk, Using dark modes for high-fidelity optomechanical quantum state transfer, New J. Phys. **14**, 105010 (2012).

[39] T. F. Roque and A. Vidiella-Barranco, Coherence properties of coupled optomechanical cavities, J. Opt. Soc. Am. B **31**, 1232 (2014).

[40] J. T. Hill, A. H. Safavi-Naeini, J. Chan, and O. Painter, Coherent optical wavelength conversion via cavity-optomechanics, Nat. Commun. **3**, 1196 (2012).

[41] Y. Liu, M. Davanco, V. Aksyuk, and K. Srinivasan, Electromagnetically induced transparency and wideband wavelength conversion in silicon nitride microdisk optomechanical resonators, Phys. Rev. Lett. **110**, 223603 (2013).

[42] C. Dong, V. Fiore, M. C. Kuzyk, and H. Wang, Optomechanical dark mode, Science **338**, 1609 (2012).

[43] S. Gröblacher, K. Hammerer, M. R. Vanner, and M. Aspelmeyer, Observation of strong coupling between a micromechanical resonator and an optical cavity field, Nature (London) **460**, 724 (2009).

[44] E. Verhagen, S. Deléglise, S. Weis, A. Schliesser, and T. J. Kippenberg, Quantum-coherent coupling of a mechanical oscillator to an optical cavity mode, Nature (London) **482**, 63 (2012).

[45] T. A. Palomaki, J. W. Harlow, J. D. Teufel, R. W. Simmonds, and K. W. Lehnert, Coherent state transfer between itinerant

microwave fields and a mechanical oscillator, Nature (London) **495**, 210 (2013).

[46] J. M. Dobrindt, I. Wilson-Rae, and T. J. Kippenberg, Parametric normal-mode splitting in cavity optomechanics, Phys. Rev. Lett. **101**, 263602 (2008).

[47] W.-J. Gu and G.-X. Li, Quantum interference effects on ground-state optomechanical cooling, Phys. Rev. A **87**, 025804 (2013).

[48] I. S. Grudinin and K. J. Vahala, Thermal instability of a compound resonator, Opt. Express **17**, 14088 (2009).

[49] C. Zheng, X. Jiang, S. Hua, L. Chang, G. Li, H. Fan, and M. Xiao, Controllable optical analog to electromagnetically induced transparency in coupled high-Q microtoroid cavities, Opt. Express **20**, 18319 (2012).

[50] B. Peng, Ş. Kaya Özdemir, F. Lei, F. Monifi, M. Gianfreda, G. L. Long, S. Fan, F. Nori, C. M. Bender, and L. Yang, Parity–time-symmetric whispering-gallery microcavities, Nat. Phys. **10**, 394 (2014).

[51] Q. Xu, S. Sandhu, M. L. Povinelli, J. Shakya, S. Fan, and M. Lipson, Experimental realization of an on-chip all-optical analogue to electromagnetically induced transparency, Phy. Rev. Lett. **96**, 123901 (2006).

[52] Y.-F. Xiao, M. Li, Y.-C. Liu, Y. Li, X. Sun, and Q. Gong, Asymmetric Fano resonance analysis in indirectly coupled microresonators, Phys. Rev. A **82**, 065804 (2010).

[53] Y. Sato, Y. Tanaka, J. Upham, Y. Takahashi, T. Asano, and S. Noda, Strong coupling between distant photonic nanocavities and its dynamic control, Nat. Photon. **6**, 56 (2012).

[54] J. Cho, D. G. Angelakis, and S. Bose, Heralded generation of entanglement with coupled cavities, Phys. Rev. A **78**, 022323 (2008).

[55] B.-B. Li, Y.-F. Xiao, C.-L. Zou, X.-F. Jiang, Y.-C. Liu, F.-W. Sun, Y. Li, and Q. Gong, Experimental controlling of Fano resonance in indirectly coupled whispering-gallery microresonators, Appl. Phys. Lett. **100**, 021108 (2012).

[56] U. Fano, Effects of Configuration Interaction on Intensities and Phase Shifts, Phys. Rev. **124**, 1866 (1961).

[57] S. E. Harris, Lasers without inversion: Interference of lifetime-broadened resonances, Phys. Rev. Lett. **62**, 1033 (1989).

[58] L. V. Hau, S. E. Harris, Z. Dutton, and C. H. Behroozi, Light speed reduction to 17 metres per second in an ultracold atomic gas, Nature (London) **397**, 594 (1999).

[59] M. D. Lukin and A. Imamoğlu, Nonlinear optics and quantum entanglement of ultraslow single photons, Phys. Rev. Lett. **84**, 1419 (2000).

[60] M. Fleischhauer, A. Imamoglu, and J. P. Marangos, Electromagnetically induced transparency: Optics in coherent media, Rev. Mod. Phys. **77**, 633 (2005).

[61] Y.-C. Liu, X. Luan, H. K. Li, Q. Gong, C. W. Wong, and Y.-F. Xiao, Coherent polariton dynamics in coupled highly dissipative cavities, Phys. Rev. Lett. **112**, 213602 (2014).

[62] J. Zheng, Y. Li, M. S. Aras, A. Stein, K. L. Shepard, and C. W. Wong, Parametric optomechanical oscillations in two-dimensional slot-type high-Q photonic crystal cavities, Appl. Phys. Lett. **100**, 211908 (2012).

[63] K. Stannigel, P. Rabl, A. S. Sørensen, P. Zoller, and M. D. Lukin, Optomechanical transducers for long-distance quantum communication, Phys. Rev. Lett. **105**, 220501 (2010).

[64] K. Stannigel, P. Rabl, A. S. Sørensen, M. D. Lukin, and P. Zoller, Optomechanical transducers for long-distance quantum communication, Phys. Rev. A **84**, 042341 (2011).

[65] S. J. M. Habraken, K. Stannigel, M. D. Lukin, P. Zoller, and P. Rabl, Continuous mode cooling and phonon routers for phononic quantum networks, New J. Phys. **14**, 115004 (2012).

[66] C. K. Law, Interaction between a moving mirror and radiation pressure: A Hamiltonian formulation, Phys. Rev. A **51**, 2537 (1995).

[67] I. Wilson-Rae, N. Nooshi, J. Dobrindt, T. J. Kippenberg, and W. Zwerger, Cavity-assisted backaction cooling of mechanical resonators, New J. Phys. **10**, 095007 (2008).

[68] E. X. DeJesus and C. Kaufman, Routh-Hurwitz criterion in the examination of eigenvalues of a system of nonlinear ordinary differential equations, Phys. Rev. A **35**, 5288 (1987).